ENERGY DEPENDENCE OF THE FRAGMENTATION OF THE AU PROJECTILE IN AU-EMULSION INTERACTIONS

A. Dąbrowska, B. Wosiek

Institute of Nuclear Physics
Kawiory 26a, 30-055 Kraków, Poland

and C.J. Waddington

University of Minnesota, Minneapolis, MN, USA

(Received November 11, 1999)

The fragmentation of gold nuclei interacting in nuclear emulsions is studied over the energy range of 0.1 to 10.6 GeV/nucleon. Different fragmentation processes are selected and investigated. The probability of fission of the gold nucleus strongly decreases with increasing beam energy. On the other hand, spallation processes do not show a significant energy dependence. At low incident energies nuclear multifragmentation only occurs in rather central Au-Emulsion interactions, while at 10.6 GeV/nucleon it is also observed in more peripheral collisions. The statistical properties of the multifragmentation events are studied. It is found that the mechanism responsible for gold multifragmentation is different than for other fragmentation processes, although no evidence suggesting the presence of a liquid-gas phase transition is found. Among Au-Emulsion interactions at 10.6 GeV/nucleon we also observe a small fraction of events in which the projectile gold nucleus is completely broken into singly charged fragments. Such events are not seen at lower energies. These interactions are the most central collisions and are accompanied by a considerable production of secondary particles.

PACS numbers: 25.75.+r, 29.40.Rg

1. Introduction

In high-energy collisions between heavy nuclei a lot of energy is available. This energy may be used to create new particles or to split both the projectile and target nuclei into nuclear fragments. In low energy collisions, $E_0 < 1$ GeV/nucleon, the process of particle production is suppressed and only in higher energy collisions can there be copious production of pions, due to interactions between the individual nucleons of the colliding nuclei. On a much longer time scale, de-excitation of the residual projectile and target nuclei occurs, accompanied by the emission of nuclear fragments. This latter process, called nuclear fragmentation, may lead to a variety of final states, characterized by different multiplicities and sizes of the fragments. For many years the process of nuclear fragmentation has been an active field of research. Despite numerous experimental and theoretical studies it is still not clearly understood. This may be explained by the fact that nuclear fragmentation is not a unique dynamical process but various underlying mechanisms come into play, leading to different fragmentation modes.

The fragmentation of gold projectiles interacting with target nuclei has been studied at energies below 1 GeV/nucleon in experiments employing several different techniques. Experiments utilizing either plastic detectors [1,2] or forward spectrometer [3] have a limited acceptance for the detection of light fragments, $Z < 6$. On the other hand more exclusive experiments using Time Projection Chambers [4, 5] detect light fragments efficiently, but are somewhat less efficient for heavier fragments. In addition, they have limited geometrical acceptance. The study presented here is based on data obtained with the nuclear emulsion technique. This technique allows for a complete detection of all projectile fragments with charge $Z \geq 1$, and is well suited to study of all the possible fragmentation channels. The principle limitations of the emulsion technique are the low event statistics and the uncertainty in the target mass assignment due to the composite nature of the emulsion target, which is a mixture of Ag, Br, O, N, and H nuclei. Nevertheless, the capability of the emulsion to record all the projectile fragments, irrespective of their charge, or emission angle, makes emulsion experiments superior, or at least competitive, for these studies, to other experimental techniques. The high energy Au-Emulsion data, presented here, were obtained by the Kraków–Louisiana–Minnesota (KLM) Collaboration, who exposed nuclear emulsion stacks to beams of gold nuclei accelerated to an energy of 10.6 GeV/nucleon at the BNL–AGS (Exp. E868) [6–12]. Lower energy data were taken by Waddington and Freier [13] at the Lawrence Berkeley Laboratory using Au nuclei from the Bevalac with an energy of 991 MeV/nucleon incident on the emulsion target.

Some results on the energy dependence of the gold projectile fragmentation have already been published by the KLM Collaboration [6, 7] showing that gold nuclei are more violently disrupted at 10.6 GeV/nucleon than below 1 GeV/nucleon. Here we present results from detailed analyses of several different modes of fragmentation. The aim of this study is to show that various underlying dynamical mechanisms are responsible for such fragmentation processes as spallation or multifragmentation. The paper is organized as follows. In the next Section we give a brief summary of the experimental details. More information on these details can be found elsewhere [7,9,12]. Section 3 discusses the fission of the gold nuclei, while Section 4 describes the energy dependence of the general characteristics of the gold fragmentation process. The studies presented in the following Sections concentrate on selected fragmentation modes, from spallation (Section 5) through multifragmentation (Section 6) up to the complete disassembly of the gold nuclei (Section 7). Section 8 presents the summary and conclusions.

2. Experimental data

A number of stacks of BR-2 nuclear emulsion pellicles were exposed at the BNL AGS to a beam of 10.6 GeV/nucleon gold ions. Gold-emulsion interactions were found by microscope scanning along the tracks produced by incident gold nuclei in order to obtain a sample with a minimum selection bias. The measured cross section for charge changing interactions was found [12] to be in reasonable agreement with the calculated charge changing cross section [14] suggesting that the scanning had an efficiency of the order of 95 ± 2 %. Those interactions that could have been missed would generally be of the sort characterized by small charge changes and low multiplicities, not multifragmentation or fission events.

Particles observed being emitted from the interactions can be divided into three categories: fragments of the target nucleus, multiply charged ($Z \geq 2$) fragments of the projectile nucleus and fast singly charged particles. Target fragments were distinguished from the projectile fragments by their low energies, in contrast to the projectile fragments, which emerge from the interactions with the same energy per nucleon as that of the incoming gold nuclei. Furthermore, target fragments are emitted nearly isotropically in the laboratory system (target at rest, or moving slowly) while projectile fragments are strongly collimated in the forward beam direction. Singly charged particles include produced particles, mostly pions, as well as singly charged projectile fragments, both spectators and participant protons. The number of singly charged projectile fragments, the so called number of released protons, although it may also include some deuterons and tritons, can be determined from charge conservation. However, these singly charged fragments cannot be separated from the produced particles on a particle-by-particle basis. It is also not possible to distinguish participant protons from the singly charged spectators emitted from the projectile. Helium fragments, on the other hand, can be readily distinguished from other fragments by their distinctive grain densities. The charges of the projectile fragments have been determined by δ-ray counts with an accuracy that is estimated to be better than 5% over the entire charge range ($Z = 3 \div 79$). The following analysis is based on a sample of 1089 gold-emulsion interactions for which the emission angles of all the particles have been measured.

We have compared these high energy interactions with a set of low energy interactions analyzed previously by Waddington and Freier [13] who exposed stacks of Ilford G5 emulsion pellicles to gold nuclei with an incident energy of 991 MeV/nucleon. At this low energy the gold nuclei are rapidly slowed down by ionization losses while traversing the emulsion medium, and can be brought to rest if they do not interact. Therefore, the energies of interacting gold nuclei ranged between the incident 991 MeV/nucleon and zero. The energy of each projectile nucleus at the interaction point was determined by range measurements. For this study only these events are considered for which the projectile energy was above 100 MeV/nucleon. The gold-emulsion interactions below 100 MeV/nucleon had an average energy of (15.6 ± 5.5) MeV/nucleon. This is close to the binding energy, and presumably these interactions tend to proceed via an intermediate composite nucleus rather than involving strong nucleon–nucleon interactions. The analyzed data set consisted of 386 interactions covering the energy from 100 to 991 MeV/nucleon. The same measurement procedures were applied as for the 10.6 GeV/nucleon data, with the exception that the emission angles were not determined.

We define for each interaction the following quantities:

N_f — number of projectile fragments with $Z \geq 3$,

N_α — number of projectile helium fragments, $Z = 2$,

N_p — number of singly charged fragments released from the projectile:

$$N_p = Z_{\mathrm{Au}} - 2 \times N_\alpha - \sum_{i=1}^{N_f} Z_i,$$

N_h — number of target fragments,

N_π — number of produced singly charged particles: $N_\pi = N_s - N_p$, where N_s is the number of singly charged minimum ionizing particles measured in each event,

Z — charge of the fragment,

Z_1 — charge of the heaviest fragment in an event,

Z_b — the sum of the charges of all fragments with $Z \geq 2$ in an event:

$$Z_b = \sum_{i=1}^{N_f} Z_i + 2 \times N_\alpha,$$

θ, φ — polar and azimuthal emission angles measured for every charged particle (available only for high energy data).

3. Fission of gold nuclei

Among the low energy gold-emulsion interactions some 7% were observed in which the projectile was broken into just two massive fragments which carried all or most of the projectile charge. These interactions were interpreted as examples of fission of the incident gold nuclei. The probability of observing an interaction with two heavy fragments Z_1 and Z_2, where $Z_1 \geq Z_2 \geq 20$ and $\mid \Delta Z \mid = Z_{\mathrm{Au}} - (Z_1 + Z_2) \leq 5$ was measured to be $(6.7 \pm 1.3)\%$. In [6,7] we reported that such interactions were practically absent in the high energy data. To confirm this observation we have performed additional scanning and found in a sample of 2177 Au-Emulsion interactions only 15 events satisfying the above selection criteria. This leads to a probability for fission-like events of $(0.69 \pm 0.18)\%$, about an order of magnitude smaller than that at low energy. The corresponding cross sections for fission of gold nuclei are 147 ± 27 mb at low energy and 19.1 ± 5.4 mb at high energy. It should be noted that emulsion scanning for fission events is 100% efficient, due to the very distinctive nature of the interaction. Hence, the observed decrease of the cross section for fission of gold projectile with increasing energy is a real effect. The same suppression of fission at high energy is also observed if the analysis is limited to symmetric fission, *i.e.* those interactions for which the asymmetry $S \leq 0.2$, where $S = (Z_1 - Z_2)/(Z_1 + Z_2)$. For symmetric fission the corresponding yields are $(4.1 \pm 1.0)\%$ at low energy and $(0.46 \pm 0.15)\%$ at high energy. We have also checked that the relative yields for fission are independent of the $\mid \Delta Z \mid$ value, for ΔZ ranging from 2 to 7. This suppression of fission at high energy is presumably due to the fact that in high-energy interactions, the projectile nuclei are excited to higher energies and other fragmentation modes, *e.g.* multifragmentation become favored. Interestingly, at the much higher energy of 158 GeV/nucleon a cross section of some 340 mb was observed for the fission of lead nuclei interacting with the lead target [15]. A large cross section for the fission of lead nuclei was also measured by the NA50 Collaboration in lead interactions with different target nuclei at 158 GeV/nucleon [16]. This large fission cross section is explained by the increased yield of Coulomb fission events. However, at energies of the order of 10 GeV/nucleon the cross section for Coulomb fission of gold nuclei is negligible, since the energy that could be transferred to the projectile via an electromagnetic excitation mechanism would be insufficient to cause fission [17].

For the following analyses the fission events, defined by $Z_1 \geq Z_2 \geq 20$ and $\mid \Delta Z \mid \leq 5$, have been excluded from both data sets.

4. Characteristics of the gold fragmentation

In order to study the energy dependence of different quantities characterizing the fragmentation of the gold nuclei, the low energy data sample has been divided into 4 subsamples, corresponding to four different energy intervals, each with approximately the same statistical weight. The 10.6 GeV/nucleon data set represents the highest energy sample in this study.

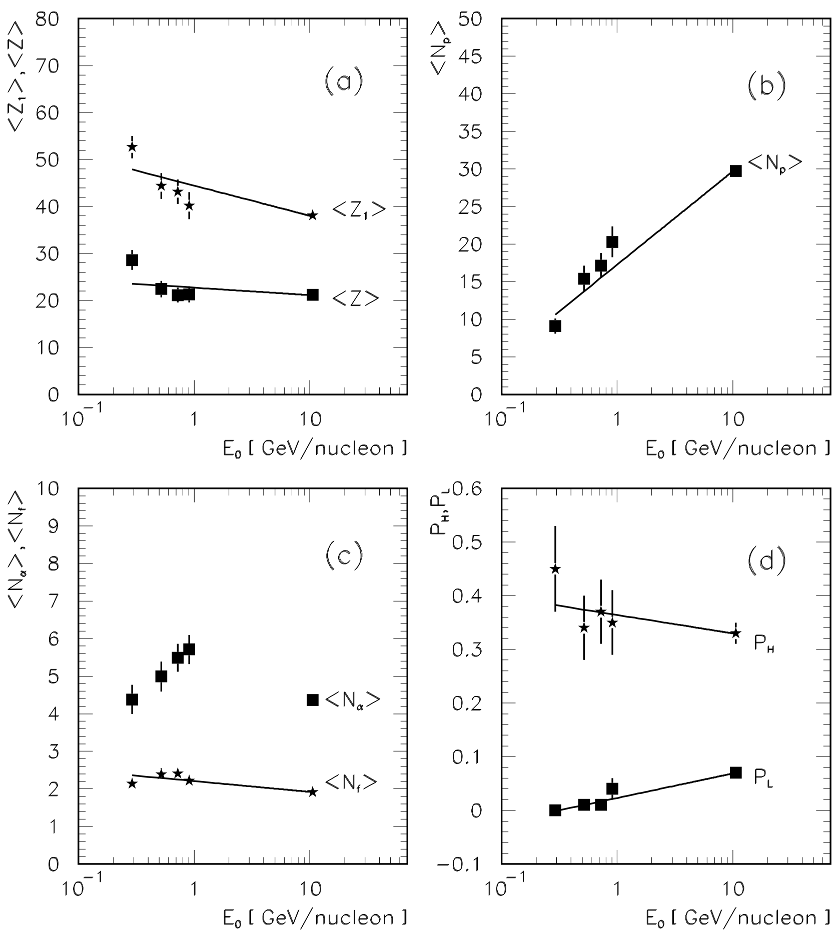

Fig. 1. Energy dependence of: (a) — mean fragment charge, $\langle Z\rangle$, and the average charge of the heaviest fragment, $\langle Z_1\rangle$; (b) — average number of released protons, $\langle N_p\rangle$; (c) — average numbers of helium, $\langle N_\alpha\rangle$, and heavier fragments, $\langle N_f\rangle$; (d) — probabilities of events with a single light fragment, P_L, and a single heavy fragment, P_H. Lines are fits to the experimental data linear in $\ln E_0$.

In Fig. 1(a) the mean charge of the fragments with $Z \geq 3$ and the mean charge of the heaviest fragment $\langle Z_1 \rangle$ are shown as a function of the incident energy. It can be seen that both $\langle Z \rangle$ and $\langle Z_1 \rangle$ decrease with increasing energy. As might be expected from charge conservation, the opposite is seen for the average number of released protons, $\langle N_p \rangle$, which strongly increases with energy (see Fig. 1(b)). The average number of fragments with $Z \geq 3$, $\langle N_f \rangle$, slightly decreases with energy (Fig. 1(c)). Also in Fig. 1(c) the increase of the mean number of helium fragments, $\langle N_\alpha \rangle$, can be observed in the energy range up to about 1 GeV/nucleon, which is not continued to higher energies. This suggests that $\langle N_\alpha \rangle$ reaches a maximum at some intermediate energy. In Fig. 1(d) we plot the energy dependence of the fractions of events with a single light fragment, P_L (events with $N_f = 1, Z \leq 15$), and with a single heavy fragment, P_H (events with $N_f = 1, Z \geq 30$) on E_0. It can be seen that P_L increases with increasing energy, while P_H decreases with increasing energy. The data on the energy dependence of $\langle Z \rangle$, $\langle Z_1 \rangle$, $\langle N_p \rangle$, $\langle N_f \rangle$, P_L and P_H all show that higher beam energy generally results in a more complete disruption of the projectile gold nuclei.

The relatively small numbers of low energy events prevents a more detailed analysis of the fragment numbers and charge distributions in restricted energy intervals. Therefore, in the subsequent studies, the low energy data sample is treated as a single set with an average energy for the interacting gold nuclei of 0.64 GeV/nucleon and a median energy of 0.62 GeV/nucleon. The average values of different measured quantities for the low and high energy data sets are listed in Table I.

TABLE I

Characteristics of gold fragmentation for low and high energy full data sets

	$\langle E_0 \rangle = 0.64$ GeV/nucleon	$E_0 = 10.6$ GeV/nucleon
N_{ev}	360	1083
$\langle N_\pi \rangle$	0.48 ± 0.13	50.53 ± 1.98
$\langle N_p \rangle$	15.94 ± 0.89	29.74 ± 0.71
$\langle N_\alpha \rangle$	5.21 ± 0.20	4.37 ± 0.09
$\langle N_f \rangle$	2.30 ± 0.08	1.91 ± 0.04
$\langle Z \rangle$	22.92 ± 0.89	21.21 ± 0.54
$\langle Z_1 \rangle$	44.62 ± 1.36	38.08 ± 0.84
$\langle Z_b \rangle$	63.06 ± 0.89	49.26 ± 0.71
$\langle Z_b^* \rangle$	-	62.83 ± 0.51

Comparison of these values reflect the systematic dependencies with energy illustrated in Fig. 1(a)–(c). One can also see that in high energy gold-emulsion interactions there is copious particle production, with an average number of created charged particles of ~ 50 per event, whereas at low energy there is little if any particle production. In Fig. 2 we plot the mean charge of fragments, $\langle Z \rangle$, with $Z \geq 3$ as a function of fragment multiplicity, N_f, for both data sets. Obviously $\langle Z \rangle$ decreases with increasing N_f due to charge conservation. However, in interactions with $N_f < 5$ we observe that, more heavy fragments are emitted at low energy than at high energy. The charge yields of N_f fragments as well as the distributions of the heaviest fragments, Z_1 have been discussed previously [7, 10].

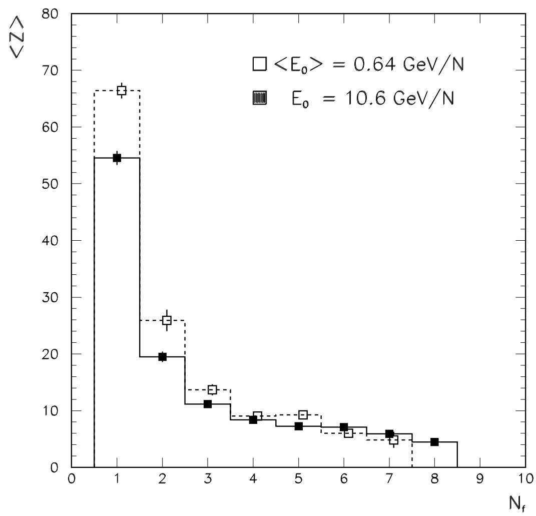

Fig. 2. Mean charge of fragments, $\langle Z \rangle$, as a function of fragment multiplicity at $\langle E_0 \rangle$ = 0.64 GeV/nucleon (open squares) and at E_0=10.6 GeV/nucleon (full squares).

The quantity Z_b, the bound charge, is related to the size of the excited projectile spectator nucleus. Therefore, it should reflect the centrality of the collision and can be used as a measure of the impact parameter; larger Z_b values should correspond to larger impact parameters and to more peripheral collisions. The size of the projectile spectator remnant is a measure of the geometry of the collision, and, therefore, for a given collision system, it should be independent of the projectile energy. Different projectile energies lead to different excitations of the spectator remnant, and ,thus, influence its decay, but not the size. Nevertheless, we do observe that $\langle Z_b \rangle$ is significantly smaller at 10.6 GeV/nucleon (see Table I) than at 0.64 GeV/nucleon. The Z_b distributions shown in Fig. 3(a) also depend on the energy. However, we defined Z_b as the sum of the charges of fragments with $Z \geq 2$, thus it is a measure of the size of the projectile spectator remnant, reduced by the number of singly charged fragments. Therefore, the above differences could be due to the energy dependence of the number of singly charged spectators which are not included in Z_b. More precisely, one can assume that at high energy larger numbers of singly charged spectators are emitted from the projectile than at lower energy. This assumption is consistent with our earlier observation of a more violent disruption of the projectile nucleus at the high beam energy, and with the observed difference in the mean number of singly charged particles released from the projectile, $\langle N_p \rangle$, see Table I. However, N_p, as it was defined in Section 2, includes both spectators and participant nucleons. The number of participants should not depend strongly on the incident energy, since in this energy range the inelastic cross section is only weakly dependent on the energy. So, the larger values of $\langle N_p \rangle$ at high energy may be explained by a larger contribution of singly charged spectators.

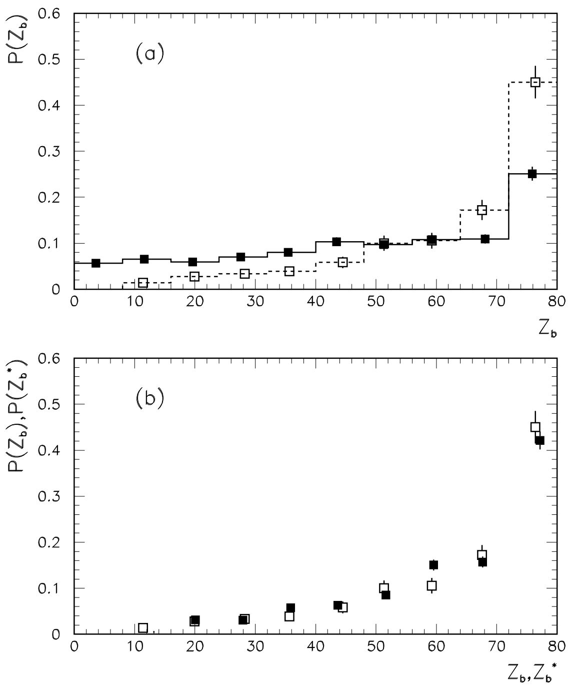

Fig. 3. (a) — Comparison of the Z_b distributions for low (open squares) and high (full squares) energy interactions. (b) — Comparison of the Z_b distribution (open squares) measured for low energy interactions and the modified (see text) Z_b^* (full squares) obtained at high energy.

We have examined this explanation for the differences observed in the Z_b distributions (Fig. 3(a)) by adding some of the N_p particles recorded in 10.6 GeV/nucleon collisions to Z_b. We make use of the fact that singly

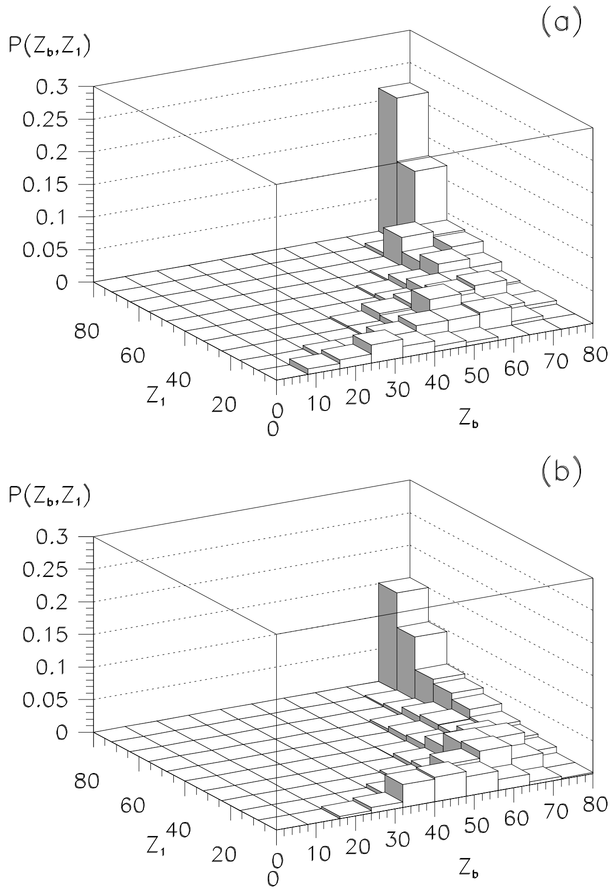

Fig. 4. Correlations between the fragment with the maximum charge observed in an event, Z_1, and Z_b at 0.64 GeV/nucleon (a) and at 10.6 GeV/nucleon (b).

charged spectators are generally emitted at smaller angles than participants, which suffered an energy loss and acquired some transverse momentum due to the interactions with target nucleons. We have selected as spectators only those singly charged particles which were emitted in a very narrow forward cone, $\theta \leq \theta_0$. For θ_0, the value of 0.0283 rad has been chosen, corresponding to 2.5 times the average emission angle for singly charged spectators ($\langle\theta\rangle = 0.12/E_0$, [18]). Then we define for high energy events a modified measure of the bound charge:

$$Z_b^* = Z_b + N_s(\theta \leq \theta_0). \quad (1)$$

The quantity $\langle Z_b^* \rangle$ defined above coincides numerically with $\langle Z_b \rangle$ measured at low energy (Table I) and the distributions, $P(Z_b^*)$ at 10.6 GeV/nucleon and $P(Z_b)$ at 0.64 GeV/nucleon are now very similar, as is shown in Fig. 3(b). Therefore, our criterion for choosing high energy spectators apparently selects, on an event-by-event basis, a fraction that is the excess over the number of spectators at low energy. Consequently we will always use Z_b^* for the 10.6 GeV/nucleon data and Z_b for the low energy data as a measure of the size of the projectile spectator, but for simplicity the superscript '*' will be omitted in what follows.

In Fig. 4 the correlation between the highest charge of fragment observed in an event, Z_1, and Z_b is shown for Au-Emulsion interactions at 0.64 GeV/nucleon (Fig. 4(a)) and at 10.6 GeV/nucleon (Fig. 4(b)). When compared to the high energy interactions those at low energy populate the region closer to the diagonal ($Z_1 = Z_b$). For the low energy data the probability that an event will have large values of both Z_1 and Z_b is much higher than at high energy. On the other hand at high energy we observe more events with a relatively light heaviest fragment ($Z_1 \leq 20$). To summarize the correlations shown in Fig. 4 provide further support for the conclusion that there is a more complete disruption of the gold nuclei at high energy than at low energy.

5. Spallation

In Section 3 we discussed one exclusive fragmentation channel, namely the fission of the gold nucleus. This process occurs in peripheral collisions where only a small amount of energy is transferred to the gold projectile (the energy threshold for fission of a Au nucleus is of the order of 55 MeV). Peripheral collisions between two nuclei may also lead to another fragmentation process, called spallation, in which only a single heavy fragment is produced. The experimental selection of the spallation process is somewhat arbitrary. There is no commonly accepted definition of what is meant by 'heavy' fragment. In general, spallation should lead to a fragment whose mass is close to the projectile mass. One can, however, also consider the so called deep spallation process which may produce a somewhat lighter fragment. Fig. 5 shows the charge spectrum for all the high energy interactions in which only one fragment with $Z \geq 3$ was emitted. Despite the large fluctuations, two distinct classes of events can be seen. In the first, at low charges, the fragment yield decreases with increasing fragment charge. In the second, at higher charges, the opposite effect is seen, with the fragment yield increasing with increasing charge. It is natural to assume that these two classes of events correspond to different fragmentation mechanisms. The behavior of the charge yield shown in Fig. 5 provides some guidance for the definition of light and heavy fragments. We assume that a heavy fragment is one with $Z \geq 30$, and consequently define spallation events as those in which

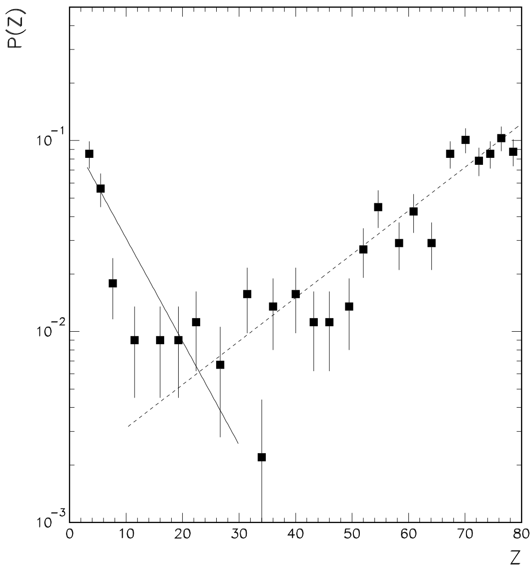

Fig. 5. Yields of fragments with $Z \geq 3$ for events with $N_f = 1$ at the energy of 10.6 GeV/nucleon. Lines are added to guide the eye to the two different classes of events.

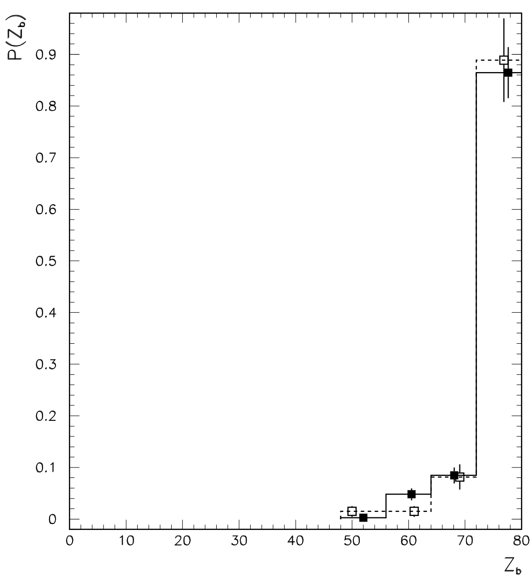

Fig. 6. Distributions of Z_b for spallation events at E_0=10.6 GeV/nucleon (full squares) and at $\langle E_0 \rangle$=0.62 GeV/nucleon (open squares).

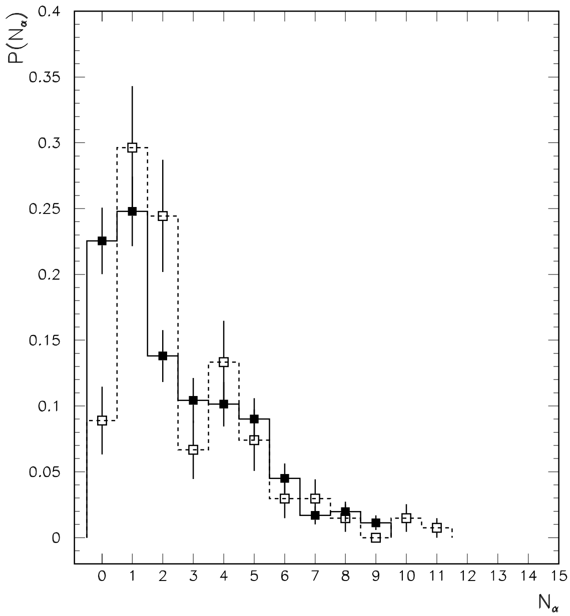

Fig. 7. Frequency distributions of the number of helium fragments, N_α, for spallation events at $\langle E_0 \rangle$=0.62 GeV/nucleon (open squares) and at E_0=10.6 GeV/nucleon (full squares).

just one ($N_f = 1$) such heavy fragment is emitted. The average characteristics of spallation interactions for the low and high energy data samples are listed in Table II. It can be seen that the probability of the nuclear spallation does not exhibit a strong energy dependence. We can conclude that for spallation the hypothesis of limiting fragmentation is validated above an energy of 0.6 GeV/nucleon. This conclusion is supported by the energy independence of the Z_b distributions for those spallation events shown in Fig. 6. The multiplicity distributions of the α particles in these events are compared in Fig. 7, and are also essentially energy independent, except at the lowest multiplicities. A comparison of the fragment charge yields, Fig. 8, shows that there are more events with very heavy fragments ($Z > 74$) at lower energy than at 10.6 GeV/nucleon. This feature is reflected in the larger value of $\langle Z \rangle$ at low energy for these spallation events than at high energy, Table II. It appears that the charge spectrum is steeper for the low energy data compared to that at high energy, although the low event statistics do not allow for a more quantified conclusion.

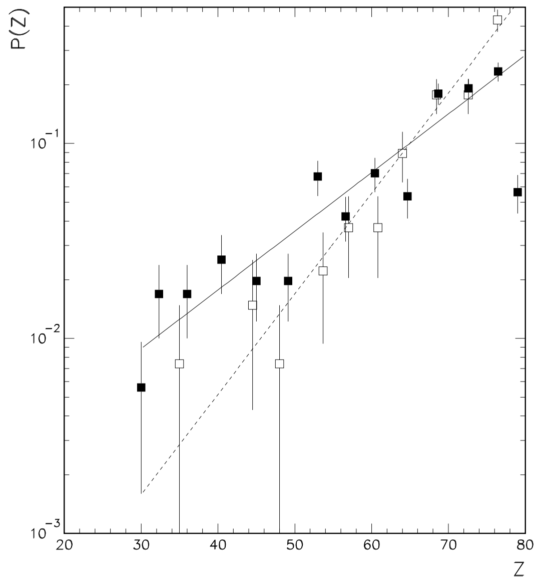

Fig. 8. Charge yields, P(Z), for spallation events as a function of Z at $\langle E_0 \rangle$=0.62 GeV/nucleon (open squares) and at E_0=10.6 GeV/nucleon (full squares). Exponential fits to each energy are shown.

TABLE II

Characteristics of gold fragmentation for low and high energy spallation events

	$\langle E_0 \rangle = 0.62$ GeV/nucleon	$E_0 = 10.6$ GeV/nucleon
N_{ev}	135	355
$p(\%)$	0.38 ± 0.03	0.33 ± 0.02
$\langle N_\pi \rangle$	0.04 ± 0.04	8.83 ± 0.55
$\langle N_p \rangle$	3.38 ± 0.41	7.81 ± 0.45
$\langle N_\alpha \rangle$	2.62 ± 0.19	2.34 ± 0.12
$\langle Z \rangle$	70.41 ± 0.67	66.53 ± 0.62
$\langle Z_b \rangle$	75.62 ± 0.41	75.96 ± 0.26

6. Multifragmentation

In more central nucleus-nucleus collisions the excited projectile remnant acquires more energy and therefore can be shattered into many small nuclear fragments. The break-up of the projectile into a large number of relatively small fragments is called multifragmentation. This process has attracted a lot of interest due to its possible relation to the liquid-gas phase transition

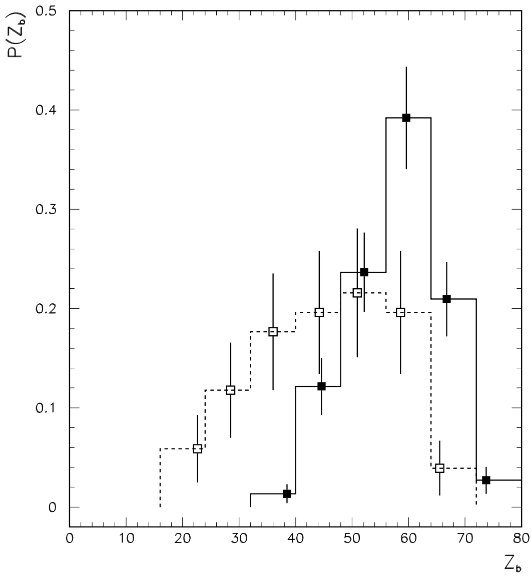

Fig. 9. Distributions of Z_b for multifragmentation events at E_0=10.6 GeV/nucleon (full squares) and at $\langle E_0\rangle$=0.71 GeV/nucleon (open squares).

TABLE III

Characteristics of gold fragmentation for low and high energy multifragmentation events.

	$\langle E_0\rangle = 0.71$ GeV/nucleon	$E_0 = 10.6$ GeV/nucleon
N_{ev}	51	148
$p(\%)$	0.14 ± 0.02	0.14 ± 0.01
$\langle N_\pi\rangle$	1.35 ± 0.56	56.78 ± 2.75
$\langle N_p\rangle$	34.25 ± 1.66	42.68 ± 0.73
$\langle N_\alpha\rangle$	9.29 ± 0.39	6.77 ± 0.20
$\langle N_f\rangle$	4.37 ± 0.16	3.82 ± 0.08
$\langle Z\rangle$	5.98 ± 0.23	5.97 ± 0.13
$\langle Z_1\rangle$	9.59 ± 0.51	9.52 ± 0.27
$\langle Z_b\rangle$	44.75 ± 1.66	57.60 ± 0.65

of nuclear matter in nuclear interactions [4,19-23]. We select this type of event from our data set by requiring the emission of more than two light fragments with $2 < Z \leq 15$. Characteristics of the selected multifragmentation events are listed in Table III for the both the low and high energy

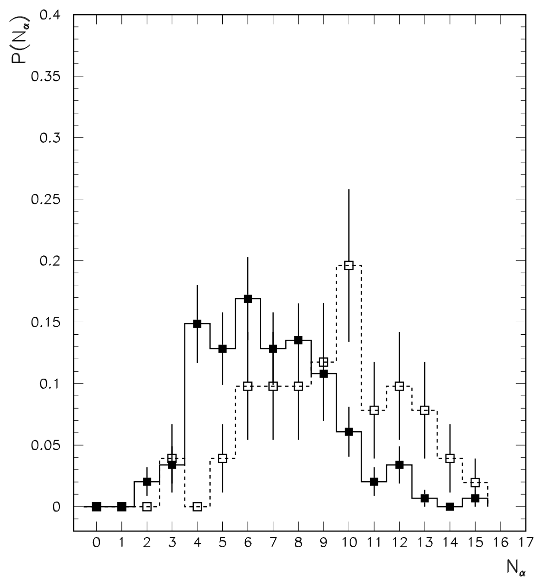

Fig. 10. Frequency distributions of the number of helium fragments, N_α, for multifragmention events at $\langle E_0\rangle$=0.71 GeV/nucleon (open squares) and at E_0=10.6 GeV/nucleon (full squares).

data. It should be noted that for the low energy data set the mean energy for multifragmentation interactions is somewhat higher than the mean energy of spallation events. The probability of multifragmentation events is $\sim$ 14%, independently of the beam energy. Unlike nuclear spallation, the characteristics of multifragmentation show a relatively strong energy dependence. The value of $\langle Z_b\rangle$ is smaller at the lower energy and more helium fragments are produced than at 10.6 GeV/nucleon. The differences shown in Table III can also be seen in the distributions of several observables. Fig. 9 compares the Z_b distributions. One can see that the high energy distribution is shifted to larger Z_b values. This indicates that at high energy, the process of multifragmentation may occur in less central collisions than at low energy. This may be due to the fact that the projectile spectator remnant is more excited at high incident energy and, therefore, even in a peripheral collision, it can acquire enough energy to undergo multifragmentation. The frequency distributions of helium fragments (Fig. 10) show an opposite tendency, with more alpha particles being emitted at low energy than at high energy.

In [22] multifragmentation has been studied for gold projectiles with energies of 200-980 MeV/nucleon. However, the plastic detector technique used in this experiment limited the analysis to fragments with charge greater than Z = 5, and thus excluded some 55% of all the light fragments

($3 \leq Z < 6$) we use to define multifragmentation.. The results of this study supported the hypothesis that multifragmentation is a statistical process. In particular it was shown that the multiplicity distributions of fragments with $6 \leq Z \leq 15$ follow a Poissonian behavior and that angular correlations in the plane perpendicular to the beam direction are consistent with the random emission of light fragments. It is interesting to see whether the same conclusions can be drawn from the analysis of all light fragments, including the most abundant ones with $Z < 6$, and if the statistical nature of multifragmentation is also valid at energies as high as 10.6 GeV/nucleon.

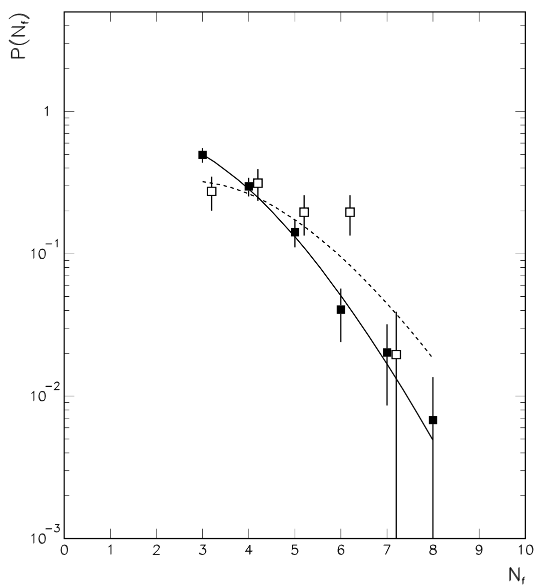

Fig. 11. Multiplicity distributions of N_f fragments for multifragmentation events with the Poisson fits at $\langle E_0 \rangle = 0.71$ GeV/nucleon (open squares) and at $E_0 =$ 10.6 GeV/nucleon (full squares).

In Fig. 11 the multiplicity distributions for fragments with $3 \leq Z \leq 15$ are shown for our multifragmentation events. They are reasonably well fitted by Poisson functions ($\chi^2/\mathrm{ndf} = 1.74$ at energies below 1 GeV/nucleon and 0.18 for 10.6 GeV/nucleon data). The distribution of the relative azimuthal angles, $\Delta\varphi$, where φ is the angle in the plane perpendicular to the beam direction, is shown in Fig. 12(a) for 10.6 GeV/nucleon fragments in multifragmentation events. This distribution is practically uniform, suggesting an isotropic emission of these fragments. In contrast the same distribution for non-multifragmentation events, selected as those in which at least two fragments with $Z > 15$ are emitted, is clearly peaked at large $\Delta\varphi$ values

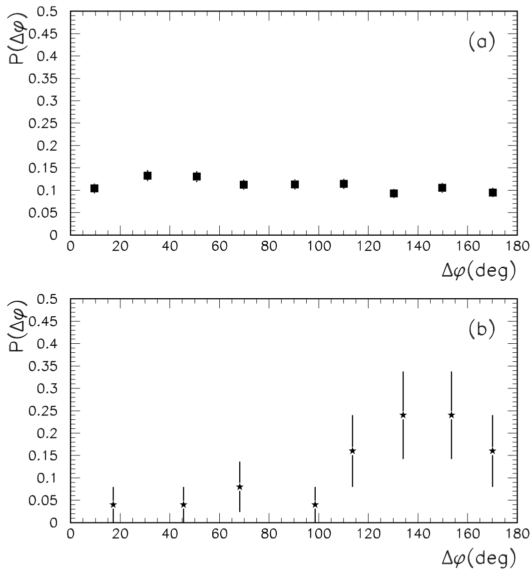

Fig. 12. Distributions for the projectile energy of 10.6 GeV/nucleon of relative azimuthal angles between fragments emitted in multifragmentation events (a), and in non-multifragmentation events (b).

(Fig. 12(b)). The azimuthal asymmetry coefficient, A, defined as

$$A = \frac{\int_0^{\pi/2} N(\Delta\varphi) d\Delta\varphi - \int_{\pi/2}^{\pi} N(\Delta\varphi) d\Delta\varphi}{\int_0^{\pi} N(\Delta\varphi) d\Delta\varphi}, \tag{2}$$

is close to zero for the multifragmentation results shown in Fig. 12(a), $A = -0.06 \pm 0.05$, in contrast to the value of $A = 0.7 \pm 0.1$, calculated for non-multifragmentation events (Fig. 12(b)). Clearly the mechanism responsible for multifragmentation is different than that involved in other fragmentation processes. This near isotropy, observed for the multifragmentation event, suggest that there are not many events in which two light fragments are emitted from some excited initial fragment, such as two Li from a C, or two Be from an O.

We have also investigated the charge correlations between the light fragments emitted in multifragmentation events. The charge correlation function is defined as

$$C(Z_1, Z_2) = \frac{\langle N_{Z_1} N_{Z_2} \rangle - \langle N_{Z_1} \rangle \langle N_{Z_2} \rangle}{\sqrt{\langle N_{Z_1} \rangle \langle N_{Z_2} \rangle}}. \tag{3}$$

The correlation function was calculated in bins of two charges for the multifragmentation events. For these events the effects due to charge con-

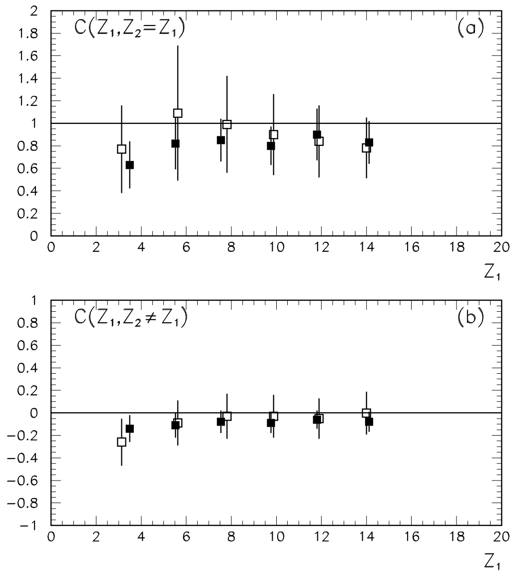

Fig. 13. Charge correlations $C(Z_1, Z_2 = Z_1)$ (a), and $C(Z_1, Z_2 \neq Z_1$ (b) as a function of Z_1 at $\langle E_0 \rangle$=0.71 GeV/nucleon (open squares) and at E_0=10.6 GeV/nucleon (full squares).

servation should be relatively minor, since the mean fragment charge (or $\langle Z_b \rangle$) is small in comparison to the projectile charge (see Table III). Therefore, if the fragment charges are statistically uncorrelated we expect that $\mathrm{C}(Z_1,\, Z_2) = 0$ for $Z_1 \neq Z_2$. The upper plot in Fig. 13 shows values of the correlation function for $Z_1 = Z_2$, which do show evidence for a correlation, for both data samples. The bottom plot presents $\mathrm{C}(Z_1,\, Z_2 \neq Z_1)$ averaged over all $Z_2 \neq Z_1$. It can be seen that indeed the $\mathrm{C}(Z_1,\, Z_2 \neq Z_1)$ values are consistent with zero (Fig. 13(b)), indicating no correlation between the fragment charges. Actually, the fact that practically all the measured values are negative reflects the presence of weak anti-correlations, due to the residual effects of charge conservation. In contrast, the diagonal elements of the correlation function, depicted in Fig. 13(a), are positive and close to unity. One would expect $\mathrm{C}(Z_1,\, Z_1) = 1$ for a Poissonian distribution of the frequency of fragments with a given charge.

The charge distributions of light fragments are compared in Fig. 14. In Fig. 14(a) the distributions are shown in a double logarithmic representation with power law fits, $P(Z) \sim Z^{-\tau}$. The fitted τ values are respectively 1.9 ± 0.1 and 1.5 ± 0.2 for the high and low energy data respectively. These values of the τ coefficients are significantly smaller than that of $\tau = 2.3$ expected when a liquid-gas transition takes place in nuclear matter [24, 25].

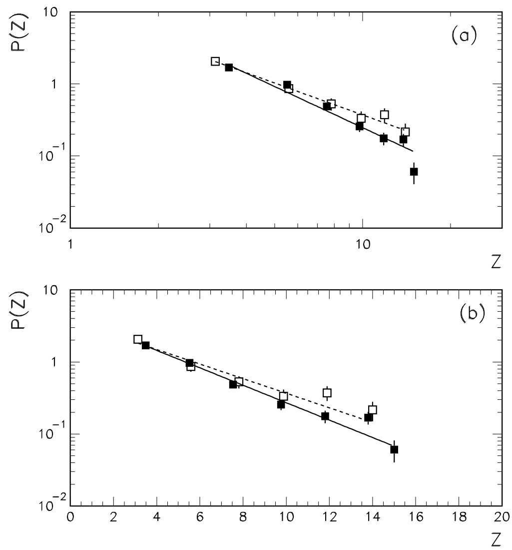

Fig. 14. Charge distributions of N_f fragments for multifragmentation events at $\langle E_0 \rangle = 0.71$ GeV/nucleon (open squares) and at $E_0 = 10.6$ GeV/nucleon (full squares). The lines are exponential (a), and power law (b) fits to the data.

It should also be noted that the quality of the power law fit is poor for the 10.6 GeV/nucleon data ($\chi^2/\mathrm{ndf} = 3.5$). Indeed, our data show that the P(Z) distributions can also be described by an exponential, $P(Z) \sim e^{-\mu Z}$, which is illustrated by a semilogarithmic representation in Fig. 14(b). The fitted values for μ are 0.28 ± 0.02 for 10.6 GeV/nucleon and 0.23 ± 0.03 for low energy multifragmentation events. Our data on the fragment charge distributions do not allow us to draw a clear distinction between the two functional forms. The power law function provides a better fit to the low energy data ($\chi^2/\mathrm{ndf} = 0.3$ as compared to $\chi^2/\mathrm{ndf} = 3.5$ for 10.6 GeV/nucleon sample), whereas the opposite is observed for the exponential fits ($\chi^2/\mathrm{ndf} = 1.9$ for low energy and 1.4 for 10.6 GeV/nucleon).

7. Total disassembly of the gold projectile

One can expect that when the projectile nucleus is excited to very high energies it may undergo a complete disruption into the smallest nuclear fragments, *i.e.* nucleons. In our low energy data we observed no events in which only singly charged particles were emitted. Note, that, since we only measure the fragment charges, this decay channel includes deuterons and tritons as well as protons. About 2 GeV of energy has to be acquired by the projectile in order to overcome the binding energy of the gold nucleus.

Either that amount of energy can not be transferred to the projectile at low beam energy, or at least the probability of such events is too low to be observed in our relatively small sample. At 10.6 GeV/nucleon the situation is kinematically more favorable and we observe $1.3 \pm 0.4\%$ of events having only singly charged fragments. These are the most central collisions of the gold projectile with heavy emulsion nuclei. They are also characterized by large target excitation (mean number of target fragments, $\langle N_h \rangle = 11.0 \pm 0.7$ as compared to the average N_h of 8.3 ± 0.3 for all gold-emulsion interactions) and large particle production. The average multiplicity of produced particles measured for these events is $\langle N_\pi \rangle = 247 \pm 11$ compared to the average of 51 ± 2 for all minimum bias events. The number of projectile spectators (defined as $N_s(\theta \leq 0.0283$ rad) is only ~ 19 per event, indicating that the majority of the projectile nucleons interacted with the target and therefore were emitted at large angles with respect to the beam direction. In Fig. 15 the pseudorapidity distribution, $dN/d\eta$ ($\eta = -\ln\tan\theta/2$), of all singly charged minimum ionizing particles for these most central events is compared to the same distribution obtained for all events in the inclusive sample of high energy. An increase of the particle production in central events is observed in the η range below $\eta \approx 5$, with the peak value exceeding $\sim$6 times the peak value measured in minimum bias Au-Emulsion collisions.

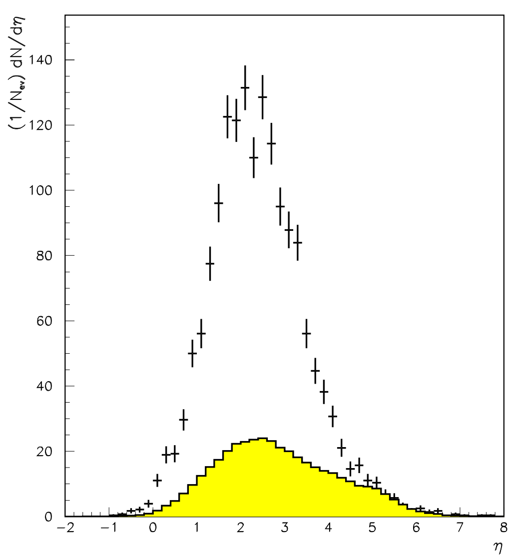

Fig. 15. Pseudorapidity distributions of singly charged particles for inclusive data (histogram) and for interactions with only singly charged fragments (crosses) at the energy of 10.6 GeV/nucleon.

8. Summary and conclusions

The fragmentation of gold projectile nuclei, interacting with target nuclei in emulsion, was studied over the energy range 0.1–10.6 GeV/nucleon.

The suppression of the fission of gold nuclei at an energy of 10.6 GeV/nucleon relative to that at lower energies, reported earlier [6,7], is confirmed on the basis of much larger event statistics.

The average characteristics of fragmentation processes other than fission, show that at high beam energy the disruption of the projectile nucleus is more severe than at low energy. Unfortunately, the low event statistics in the energy ranging from 0.1–1 GeV/nucleon prevented a detailed, systematic study of various fragmentation processes as a function of primary energy. As a result the analysis of different fragmentation channels was limited to two samples of Au-Emulsion interactions, a high energy sample and a low energy sample. For this low energy sample the incident energies ranged from 0.1 to 1 GeV/nucleon, with an average energy of 0.64 GeV/nucleon.

Spallation processes leading to the emission of a single heavy fragment ($Z \geq 30$) do not show a significant energy dependence. These processes constitute about 35% of all events and are assumed to represent peripheral Au-Emulsion interactions.

In more central collisions the emission of several relatively light fragments from the excited projectile remnant is observed. These, so called multifragmentation processes were selected by requiring the presence of at least three fragments with charges $3 \leq Z \leq 15$. They represent about 14% of all events irrespectively of the primary energy. The comparison of the distributions of the total charge bound in the projectile remnant shows that at high energy the multifragmentation processes occur in less central interactions than in the low energy interactions. This suggests that the projectile nucleus can be excited to higher energies at high beam energy. Detailed analysis of multifragmentation events shows that they can be explained by assuming a statistical probability for the emission of the fragments. In particular fragment frequency distributions are found to be consistent with a poissonian spectrum and no correlations between fragment charges are observed. Furthermore, the distribution of the relative angles in the plane perpendicular to the beam axis supports the hypothesis of isotropic fragment emission. These observations and the results of the study of charge yields in multifragmentation events provide no evidence for the presence of a liquid-gas phase transition.

At high beam energy we observe events in which the energy transferred to the gold projectile is sufficient to cause its breakup into the smallest nuclear pieces, hydrogen, deuterium and tritium nuclei. In about 1% of the interactions recorded at 10.6 GeV/nucleon we observe only singly charged fragments being emitted from the projectile nuclei. These are the most central collisions in which there is also a copious production of secondary particles. On average about 250 particles are produced in events with $N_f = N_\alpha = 0$, *i.e.* 5 times more than in the minimum bias events.

The effort of all our colleagues from the KLM Collaboration put to the scanning, and measurements of the 10.6 GeV/nucleon interactions is gratefully acknowledged. We thank the staff of the Bevalac and the AGS for assistance in making these exposures. This work was partially supported in Poland by the State Committee for Scientific Research Grant 2P03B05417. C.J.W. is partially supported by NASA under Grant NASA/NAS5-5113.

REFERENCES

[1] J. Dreute *et al.*, *Phys. Rev.* **C44**, 1057 (1991).
[2] S. E. Hirzebruch *et al.*, *Phys. Rev.* **C51**, 2085 (1995).
[3] J. Hubele *et al.*, *Z. Phys.* **A340**, 263 (1991).
[4] A.S. Hirsh *et al.*, *Phys. Rev.* **C29**, 508 (1994).
[5] M. Gilkes *et al.*, *Phys. Rev. Lett.* **73**, 1590 (1994).
[6] C.J. Waddington, Int. J. Mod. Phys. **E2**, 739 (1993).
[7] M.L. Cherry *et al.*, *Z. Phys.* **C62**, 25 (1994).
[8] M.L. Cherry *et al.*, *Z. Phys.* **C63**, 549 (1994).
[9] M.L. Cherry *et al.*, *Phys. Rev.* **C52**, 2652 (1995).
[10] M.L. Cherry *et al.*, *Phys. Rev.* **C53**, 1532 (1996).
[11] M.L. Cherry *et al.*, *Z. Phys.* **C73**, 449 (1997).
[12] M.L. Cherry *et al.*, *Eur. Phys. J.* **C5**, 641 (1998).
[13] C.J. Waddington, P.S. Freier, *Phys. Rev.* **C31**, 888 (1985).
[14] B.S. Nilsen *et al.*, *Phys. Rev.* **C52**, 3277 (1995).
[15] M.L. Cherry *et al.*, *Acta Phys. Pol.* **B29**, 2155 (1998).
[16] M.C. Abreu *et al.*, *Phys. Rev.* **C59**, 876 (1999).
[17] C.F. Weizsäcker, *Z. Phys.* **88**, 612 (1934); E.J. Williams, *Phys. Rev.* **45**, 729 (1934); J.D. Jackson, *Classical Electrodynamics*, Wiley, NY, 1975.
[18] C.F. Powell, P.H. Fowler, P.H. Perkins, *The Study of Elementary Particles by the Photographic Method*, Pergamon Press, 1959.
[19] X. Campi, *Phys. Lett.* **B208**, 351 (1988).
[20] X. Campi, *J. Phys.* **A19**, 917 (1986).

[21] B. Jakobsson *et al.*, *Nucl. Phys.* **A509**, 159 (1990).
[22] C. Lewenkopf *et al.*, *Phys. Rev.* **C44**, 1065 (1991).
[23] C.A. Ogilvie *et al.*, *Nucl. Phys.* **A533**, 271c (1993).
[24] M.E. Fisher, *Physics* (N.U.) **3**, 255 (1967).
[25] A.D. Panagiotou *et al.*, *Phys. Rev. Lett.* **52**, 496 (1984).